# Journal of Materials Chemistry B

Accepted Manuscript






ROYAL SOCIETY OF CHEMISTRY

www.rsc.org/materialsB

Cite this: DOI: 10.1039/c0xx00000x

www.rsc.org/xxxxxx

ARTICLE TYPE

# Synthesis of SBA-15 Rods with Small Sizes for Enhanced Cellular Uptake

**Yannan Yang, [a‡] Surajit Karmakar,[a‡] Jun Zhang,[a] Meihua Yu,[a] Neena Mitter,[b] and Chengzhong Yu*[a]**

***Received (in XXX, XXX) Xth XXXXXXXXX 20XX, Accepted Xth XXXXXXXXX 20XX***

**DOI: 10.1039/b000000x**

Small sized SBA-15 rods with 80-200 nm in length, 18±8 nm in width and pore size of 8.3 nm have been successfully synthesized by finely tuning the synthesis pH in a narrow range of 3.40-3.88. Compared to traditional SBA-15 with relatively larger particle sizes and MCM-41 with smaller pore sizes, SBA-15 rods prepared in this study demonstrate higher adsorption capacity towards large protein molecules such as bovine serum albumin and lysozyme, and enhanced cellular uptake efficiency in human osteosarcoma cancer cells. This novel silica material with small particle sizes, large pores as well as excellent biocompatibility is a promising delivery system for the cellular delivery of large molecular weight therapeutic agents with improved efficacy.

## 1. Introduction

In recent decades, the development of nanomaterials has profoundly affected nanomedicine in the field of disease diagnosis and therapy.[1] Among various nanomaterials, mesporous silica nanoparticles (MSNs) have been regarded as promising nanocarriers for the cellular delivery of therapeutic or diagnostic agents due to their versatile and controlled pore structures, particle size, morphology and surface functionality.[2, 3] MCM-41[4] is the most extensively studied type of MSNs because their particle sizes can be efficiently controlled in the range of 30-200 nm,[5] which is beneficial for cellular uptake and subsequent bio-applications.[6] The pore size of MCM-41 type MSNs is generally less than 5 nm.[7] Compared to MCM-41, SBA-15[8] type MSNs have larger pore sizes (5-30 nm), which have been utilized as efficient nanocarriers to accommodate and deliver large molecules, such as therapeutic proteins.[9-11] However, the particle sizes of SBA-15 used were in the range of 800 nm - 2 µm, larger than the satisfactory requirement of sufficiently small particle size (< 200 nm) for efficient cellular uptake.[2, 5] In addition, SBA-15 silica materials with large particle sizes have limitation in large molecular diffusion and adsorption capacity.[12] Thus, the development of small sized SBA-15 is in great demand for enhanced cellular delivery of large molecules.

To date, much effort has been made to control the particle size of SBA-15 silica materials. The most typical morphology for SBA-15 is rods with sizes in micrometer range.[13, 14] Nazar et al. successfully reduced SBA-15 with 10 porous channels in width and 300 to 600 nm in length by reducing surfactant and silica source concentrations.[15] Lu et al. developed monodispersed SBA-15 with a length of 300-400 nm by tuning the concentration of hydrochloride acid (HCl) in the presence of glycerol, which exhibited rapid lysozyme immobilization and high adsorption capacity due to the short length. Johansson et al. reported SBA-15 rods with variable length (400-600 nm) and width (100-400 nm) by varying the HCl concentration in the presence of heptane and $NH_4F$.[16] Recently, Yin et al. reported a convenient route to prepare rodlike SBA-15 with varying lengths (600-3000 nm) and widths (260-400 nm).[17] However, it is still a challenge to synthesize SBA-15 with length less than 200 nm and width less than 50 nm with highly efficient cellular uptake performance.

Herein, we report a facile approach to synthesize small SBA-15 rods with 80-200 nm in length and 18±8 nm in width by precisely controlling the synthesis pH values in a small range of 3.40-3.88. Compared with traditional SBA-15 and MCM-41 silica materials, the obtained small SBA-15 rods with a large pore size of 8.3 nm and excellent dispersity show enhanced protein adsorption capacity towards bovine serum albumin and lysozyme, and improved cellular uptake performance. To the best of our knowledge, the SBA-15 rods prepared in our system have the smallest particle size among those have been reported so far.

## 2. Experimental section

### 2.1 Chemicals

Tetraethylorthosilicate (TEOS), tetramethoxyorthosilicate (TMOS), cetyltrimethylammonium bromide (CTAB), (3-aminopropyl) triethoxysilane (APTES), rhodamine B isothiocyanate (RB), poly(ethylene oxide)-poly(propylene oxide)-poly(ethylene oxide) block copolymer ($PEO_{20}$-$PPO_{70}$-$PEO_{20}$, known as Pluronic®P123), bovine serum albumin (BSA) and lysozyme (LYS) were purchased from Sigma-Aldrich. Reagent grade sodium hydroxide (NaOH) and hydrochloric acid (HCl) were received from ChemSupply and Ajax Finochem Pty Ltd, respectively. Ethanol was purchased from RCI Labscan Ltd. CellTiter-Blue®Reagent was ordered from Promega. Human osteosarcoma KHOS cell line was purchased from American Type Culture Collection.

### 2.2 Synthesis of SBA-15 like rods

In a typical process, 1.0 g of P123 was added to 30 ml of HCl aqueous solution with different pH (pH = 3.40, 3.68, 3.76, 3.88). The mixture was stirred at 30 °C until the polymer was dissolved completely. Then, 2.38 ml of TMOS was added to this solution under vigorous stirring. After 10 min of stirring, the mixture was kept under static conditions at 30 °C for 24 h. Then the mixture was transferred to an autoclave for hydrothermal treatment at 100 °C for 24 h. The resultant white precipitates were filtered, washed and then dried in air. Surfactants were removed by extraction in acidic ethanol at 60 °C for 8 h. The solvent extraction process was repeated three times to completely remove the surfactant. The final samples were denoted SR-X, where SR indicates SBA-15 rods and X represents the synthesis pH value.

### 2.3 Synthesis of MCM-41

MCM-41 was synthesized according to an approach reported in literature[18] with slight modifications. In a typical synthesis, 1.0 g CTAB was dissolved in 480 g deionized water under stirring at room temperature followed by the addition of 3.5 mL NaOH (2 M).The temperature of the solution was raised and kept at 80 °C. To this solution, 6.7 mL TEOS was added. The mixture was continuously stirred for an additional 2 h. The resultant products were collected by filtration and dried at room temperature. The templates were removed by the solvent extraction process as mentioned above.

### 2.4 Amino and RB functionalization

In a typical amino modification process, 150 mg of SR-3.40, SR-3.88 or MCM-41 were mixed with 6 ml toluene and sonicated for 10 min before adding 0.l ml APTES. After stirring at 110 °C for 12 h, the products were extensively washed with toluene and ethanol, and dried in a fume-hood at room temperature. In order to modify particles with RB, 20 mg amino functionalized SR-3.40, SR-3.88 or MCM-41 were dispersed in 3 ml deionized water, and mixed with 5ml RB ethanol solution (0.3 mg/ml). After stirring in the dark at room temperature for 6 h, the products were centrifuged and washed with ethanol three times until the supernatants were colorless. The samples were denoted as RB-SR-3.40, RB-SR-3.88 and RB-MCM-41.

### 2.5 Characterization

Scanning electron microscopy (SEM) was performed on a scanning electron microscopy (type HITACHI S-4800) with an accelerating voltage of 3 kV. Transmission electron microscopy (TEM) images were obtained with a JEOL 2100 operated at 100 kV. For TEM measurements, the samples were prepared by dispersing the powder samples in ethanol, after which they were dispersed and dried on carbon film on a Cu grid. The X-ray diffraction (XRD) pattern was recorded on a Rigaku Miniflex X-ray diffractometer with Ni-filtered Cu Kα radiation (λ= 1.5406 Å). Nitrogen adsorption–desorption isotherms were measured at 77 K using a Micromeritics ASAP Tristar II 3020 system. The samples were degassed at 453 K overnight on a vacuum line. The pore size distribution curve was derived from the adsorption branch of the isotherm using the Barrett–Joyner–Halanda (BJH) method. The Brunauer–Emmett–Teller (BET) method was utilized to calculate the specific surface areas. The total pore volume was calculated from the amount adsorbed at a maximum relative pressure ($P/P_0$) of 0.99.

### 2.6 Protein adsorption

For the adsorption of BSA or LYS to the SBA-15 rods and MCM-41, protein was first dissolved in phosphate buffer solution (PBS, 0.1 M, pH 7.4) to obtain a protein stock solution with a concentration of 2 mg $ml^{-1}$. PBS buffer solution (0.75 ml) was added to 1.5 mg of the silica particles in 2 ml capped vials. After the mixture was sonicated for 10 min, 0.75 ml of protein stock solution was added. The total volume and concentration of protein solution were 1.5 ml and 1 mg $ml^{-1}$, respectively. The resulting mixture was shaking at 200 rpm at room temperature for 6 h. The amount of protein adsorbed to the silica particles was further quantified by measuring the absorbance of the supernatant at 280 nm. The amount of protein adsorbed was calculated by the concentration difference between before and after adsorption.

### 2.7 Cell studies

**Cell culture:** KHOS cells were propagated in a monolayer to sub-confluency at 37 °C in 75 $cm^2$ flasks containing 10 ml of Dulbecco's Modified Eagle Medium (DMEM), supplemented with heat inactivated 10% fetal calf serum (FCS), 1% penicillin, 1% glutamine and 1% streptomycin in a fully-humidified incubator containing 5% $CO_2$ and 95% air.

**Cellular uptake assay:** $2\times10^5$ KHOS cells per well were seeded on cover glass in 6 well-plates and incubated overnight. Next day, cells were treated with the Rhodamine B-labelled nanoparticles (RB-SR-3.40, RB-SR3.88 and RB-MCM-41) at 50 µg/ml concentration for 4 h in serum-free medium. Following completion of treatment, plates were washed with PBS for 2 times and cells were fixed with 4% paraformaldehyde for 15 minutes and washed with PBS. Nuclei were stained with a DAPI mount solution (Sigma-Aldrich, Australia) on glass slides. The uptake performance of nanoparticles was assessed using a confocal microscopy (LSM710, Zeiss).

**Detection of inductively coupled plasma optical emission spectrometry (ICP-OES):** To quantitatively compare cellular uptake of different silica nanoparticles, $5\times10^5$ KHOS cells per well were seeded in a 6 well-plates and cultured for 24 h. Under serum free condition, cells were incubated with nanoparticles (50 µg/ml) for 4 hours followed by washing with PBS and harvested with trypsin. After centrifugation, the cell pellets were washed twice with PBS and number counting were done, then again centrifuged and dried overnight. Cells were sonicated using cell lysis buffer (Cell Signaling Technology) and the supernatants (containing cell components) were removed by centrifugation at 13,000 rpm for 10 minutes, followed by two washes with PBS. Aqueous NaOH solution (1 M) was then added to allow dissolution of the nanoparticles with ultrasound sonication. The silicon concentrations in the final solutions were measured by Inductively Coupled Plasma Optical Emission Spectrometer (ICPOES) with a Vista-PRO instrument (Varian Inc, Australia) and the number of internalized nanoparticles was determined. All experiments were performed in triplicate.

**MTT (3-[4,5-dimethylthiazol-2-yl]-2,5 diphenyl tetrazolium bromide) assay:** The sensitivity of KHOS cells to the nanoparticles were determined by the MTT colorimetric assay. Cells ($1\times10^4$ per well) were seeded in a flat-bottomed 96-well plate and incubated at 37 °C and in 5% $CO_2$. Cells were exposed

to nanoparticles in a dose dependent manner for 24 h. Following treatment completion, cells were incubated with MTT reagent (10 µl/well volume from 5 mg/ml solution in PBS) for 4 h at 37 °C. Then dimethyl sulfoxide (DMSO) (100 µl) was added to each well and mixed to dissolve the formazan crystal. The optical density (OD) was recorded at 570 nm in a microplate reader and the percentage of residual cell viability was determined. All experiments were performed in triplicate.

## 3. Results and discussion

### 3.1 Synthesis and characterization of SBA-15 rods

The XRD patterns of samples SR-X (X = 3.40, 3.68, 3.76, 3.88) are shown in Fig. 1. For SR-3.4, three well-resolved diffractions appear at 2θ = 1.00, 1.68 and 1.92 with a 1/*d* ratio close to 1: √3:2, which can be indexed as the 100, 110, and 200 reflections of a highly ordered two dimensional (2D) hexagonal mesostructure (p6mm).[8] The $d_{100}$ spacing was calculated to be 8.8 nm (Table 1), corresponding to a unit cell parameter ($a_0$) of 10.2 nm. The XRD patterns of the rest SR are similar to that of SR-3.4. However, the 100 peak position gradually shifts to a smaller angle when the pH increases from 3.68 to 3.88, indicating an increase of $d_{100}$ spacing (Table 1). It is notable that the full width at half maximum (FWHM) of the 100 peaks is broadened from 0.15 to 0.47 degree when increasing the pH from 3.40 to 3.88, suggesting a decrease in average particle size.[19]

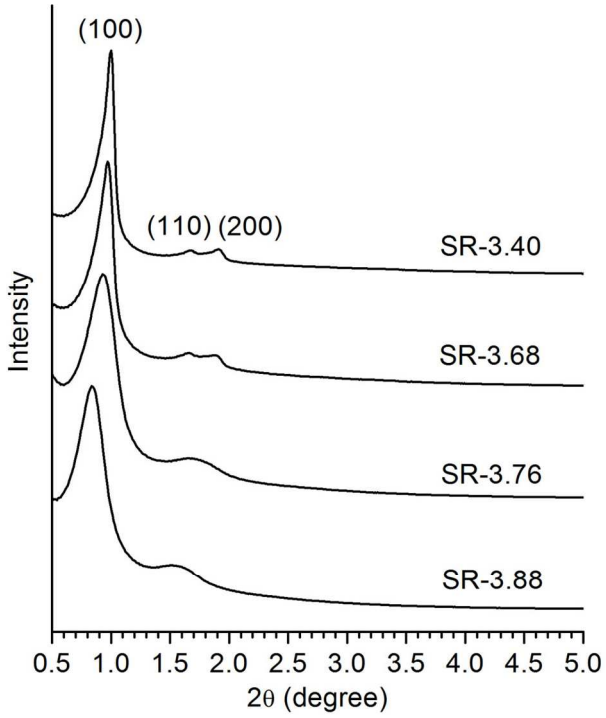


**Fig. 1** XRD patterns of samples SR-X (X = 3.40, 3.68, 3.76, 3.88).

The morphologies and the structures of samples SR-X (X = 3.40, 3.68, 3.76, 3.88) were investigated by SEM and TEM. From the SEM images (Fig 2a, d, j, g), it can be seen that all the samples have a rod like morphology while both the length and width of the rods decreases from micrometer size to a few hundred nanometers as the pH value increases from 3.40 to 3.88. The TEM image reveals that SR-3.40 has a length of 0.78-1.5 µm and width of 220-350 nm (Fig. 2b), displaying a typical pattern viewed along the [110] direction of a 2D hexagonal structure (Fig. 2c). When the pH increases to 3.68, there is no obvious change in the length of rods for the sample SR-3.68, but the width decreases to 100-140 nm (Fig. 2e). The ordered mesopores within the rods can be clearly seen from the magnified TEM image (Fig. 2f). When pH value further increases to 3.76, the length and width of sample SR-3.76 significantly decreases to 100-350 nm and 30-50 nm, respectively (Fig. 2h). Only a few (~ 4-6) packed cylindrical meso-channels along the long axis of the rods can be seen (Fig. 2i). By further slightly increasing pH to 3.88, well dispersed rods with even smaller sizes were obtained with 80-200 nm in length and 18±8 nm in width (Fig. 2k). The high magnification TEM image (Fig. 2l) clearly reveals sample SR-3.88 has only 2-4 cylindrical mesopores. The trend of decreased particle size from pH 3.40 to pH 3.88 observed in SEM and TEM is in good accordance with the XRD results. Theoretically, a number of three parallel meso-channels viewed along the [110] direction is the smallest possible constitution that makes a perfect hexagonal symmetry. The observation of two meso-channels in Fig. 2k&l indicates that the synthesis pH of 3.88 is a critical point in our system to prepare SBA-15 type MSNs with the smallest size.

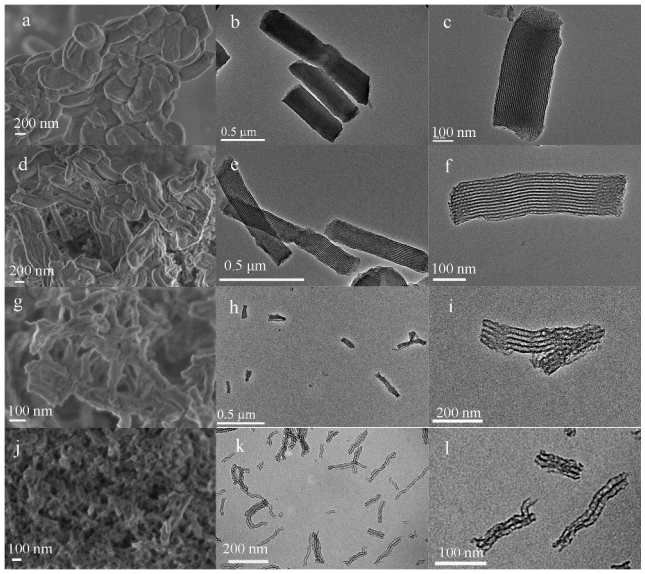


**Fig. 2** SEM (a, d, g, j) and TEM images of sample SR-3.40 (b, c), SR-3.68 (e, f), SR-3.76 (h, i), SR-3.88 (k, l), respectively.

The nitrogen adsorption-desorption isotherms (Fig. 3a) of these four SR-X samples are typical type IV in all cases. For the sample SR-3.40, a steep capillary condensation step occurs at a relative pressure ($P/P_0$) of ~ 0.7, corresponding to a narrow pore size distribution centred at 7.0 nm (Fig. 3b). As the pH value increases from 3.40 to 3.88, the steep capillary condensation step gradually moves to a higher $P/P_0$ from 0.70 to 0.76, indicative of enlarged pore sizes. The pore size calculated for sample SR-3.68, SR-3.76 and 3.88 is 7.1, 7.5 and 8.3 nm, respectively (Fig. 3b). The pore diameters, surface areas and pore volumes of four samples are summarized in Table 1 for comparison. It is notable that SR-3.88 with the smallest particle size among those samples exhibits the highest surface area, largest pore volume and pore size, which are beneficial for efficient adsorption of large guest

molecules.

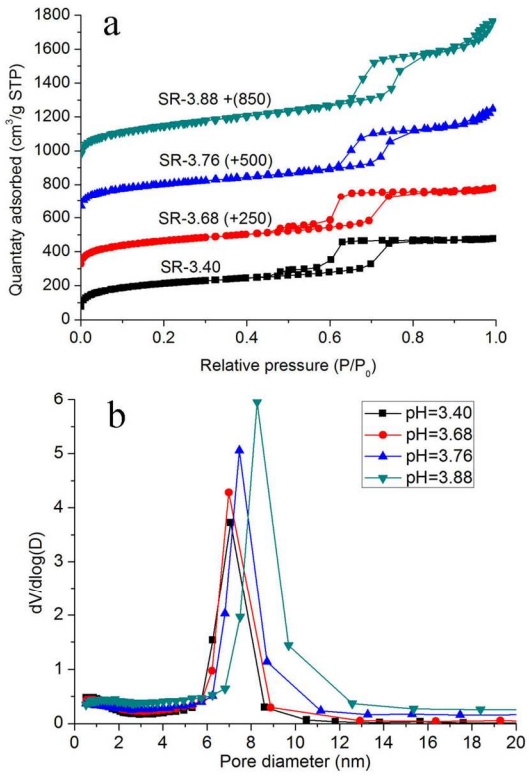


**Fig. 3** (a) $N_2$ sorption isotherms and (b) BJH pore size distribution curves of SR-X (X = 3.40, 3.68, 3.76, 3.88).

The pore size of SBA-15 is mainly determined by the size of hydrophobic core of block copolymer templates.[20] When pH increases, the protonation degree of PEO chain decreases, leading to enlarged hydrophobic core sizes. [21] Therefore, as pH increases from 3.40 to 3.88, the pore size of SR-X increases from 7.0 to 8.3 nm. When the synthesis pH is above the critical point of 3.88, silica vesicles with a size of ~ 80 nm mixed with a few tubular structures are obtained when the pH is increased slightly to 3.98 (Fig. S1). The pore diameter of tubular silica is estimated to be ~ 9.0 nm, which is close to the cylindrical pore diameter of SR-3.88. Moreover, generally one single tube is observed, rather than more than two meso-channels packed together in SR-X samples. The structural transition from a hexagonal mesostructure to multi-lamellar vesicles induced by increased pH has been reported,[22 23] which can be explained by increased hydrophobicity due to decreased protonation of EO moieties. Our results reveal that this structure transition is very sensitive to pH: a small increase from 3.88 to 3.98 triggers a significant change from rod-like morphology to vesicles. Compare to the previous reports, in this study we focus on the morphology evolution right before the structural transition occurs. By systematically tuning the synthesis pH values in a small range (3.40-3.98), the sensitive point (pH=3.88) is identified where the smallest SBA-15 type MSNs (mixed with even smaller particles which should not be called SBA-15) are prepared. It is proposed that the decrease in the number and length of meso-channels from pH 3.40 to 3.88 is also associated with the trend in structural transition, favouring the formation of vesicular structures when the pH exceeds the critical point.

**Table 1** Structural properties of samples SR-X (X = 3.40, 3.68, 3.76, 3.88).

| Sample name | $d_{100}$ spacing (nm) | $D_p$ (nm) | $S_{BET}$ ($m^2 g^{-1}$) | $V_t$ ($cm^3 g^{-1}$) |
|---|---|---|---|---|
| SR-3.40 | 8.8 | 7.0 | 707 | 0.75 |
| SR-3.68 | 9.1 | 7.1 | 724 | 0.83 |
| SR-3.76 | 9.5 | 7.5 | 694 | 1.01 |
| SR-3.88 | 10.6 | 8.3 | 867 | 1.32 |

$D_p$: the pore diameter calculated from the adsorption branch of the isotherm using the BJH method; $S_{BET}$: specific surface area; $V_t$: the total pore volume at relative pressure 0.99.

### 3.2 Protein adsorption

Both the pore sizes and particle sizes are important structure parameters of MSNs for their protein adsorption capacity. For comparison MCM-41 rods were synthesized to compare with SR-3.40 and SR-3.88. The obtained MCM-41 has a hexagonal pore symmetry, particle size of 50-100 nm and pore size of 2.3 nm (as demonstrated in Fig. S2). Bovine serum albumin (BSA) with a large molecular size (5.0×7.0×7.0 nm)[24] and lysozyme (LYS) with a smaller size (1.5×2.5×4.3 nm)[24] were selected as the model protein molecules. The protein adsorption capacity of these silica materials was evaluated at pH 7.4 in PBS solution. As shown in Fig. 4, SR-3.88 exhibits the highest loading capacity towards BSA (438 mg $g^{-1}$) and LYS (417 mg $g^{-1}$) among three silica materials. SR-3.40 shows a relatively lower adsorption capacity of 180 mg $g^{-1}$ and 219 mg $g^{-1}$ for BSA and LYS, respectively. Compared to SR-3.88, although SR-3.40 has a similar pore size, the larger particle size hence longer channel length may limit the diffusion and access of protein molecules into the pores,[25, 26] causing a smaller loading capacity. As expected, MCM-41with a pore size (2.3 nm) smaller than the protein size displays an extremely low adsorption capacity towards BSA (5 mg $g^{-1}$), where only external surface was utilized for BSA adsorption. In the case of LYS, MCM-41 shows a higher adsorption capacity of 189 mg $g^{-1}$ compared to that of BSA because the pore size of

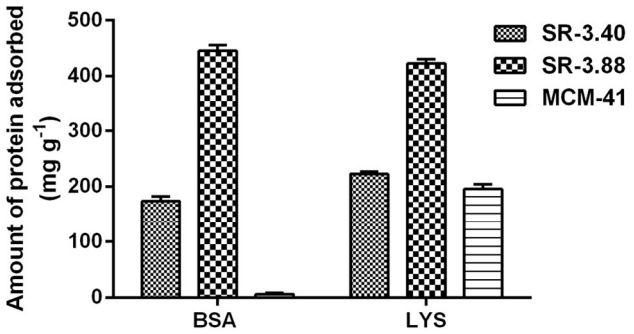


**Fig. 4** BSA and LYS adsorption capacity of SR-3.40, SR-3.88 and MCM-41

MCM-41 is close to the LYS molecular size, thus LYS could be loaded on the external surface and internal pores. However, the LYS loading capacity of MCM-41 is the smallest among three materials under study similar to literature findings.[27] Our results indicate that both large pore sizes and small particle sizes are crucial for efficient adsorption of various large protein molecules.

### 3.3 Cellular uptake and biocompatibility

Besides high loading capacity, enhanced cellular uptake performance of nano-carriers is also important to achieve high efficiency for their cell based applications. We further investigated the cellular uptake performance of SR-3.40, SR-3.88 and MCM-41 in human osteosarcoma cancer cells (KHOS). To

monitor the silica nanoparticles entered into cells, rhodamine-B (RB) labelled SR-3.40 (RB-SR-3.40), SR-3.88 (RB-SR-3.88) and MCM-41 (RB-MCM-41) were synthesized. The KHOS cells treated with three different fluorescent silica materials were studied by confocal laser scanning microscopy (CLSM). As shown in Fig. 5, only the nuclei are observed in blue colour after staining with DAPI for the cells without any treatment (Fig. 5a). When the cells treated with RB labelled silica materials, red signal (RB) can be detected inside the cells (Fig. 5 b-d), indicating that the silica materials are readily taken up by KHOS cells. However, the red fluorescence intensity of cells incubated with RB-SR-3.40 (Fig. 5b) is weaker than those cells incubated with RB-SR-3.88 (Fig. 5c) and RB-MCM-41 (Fig.5d), suggesting less amount of RB-SR-3.40 internalized by KHOS cells compared to the other two silica materials. The significantly enhanced cellular uptake efficiency of RB-SR-3.88 and RB-MCM-41 was attributed to their small particle sizes.[5]

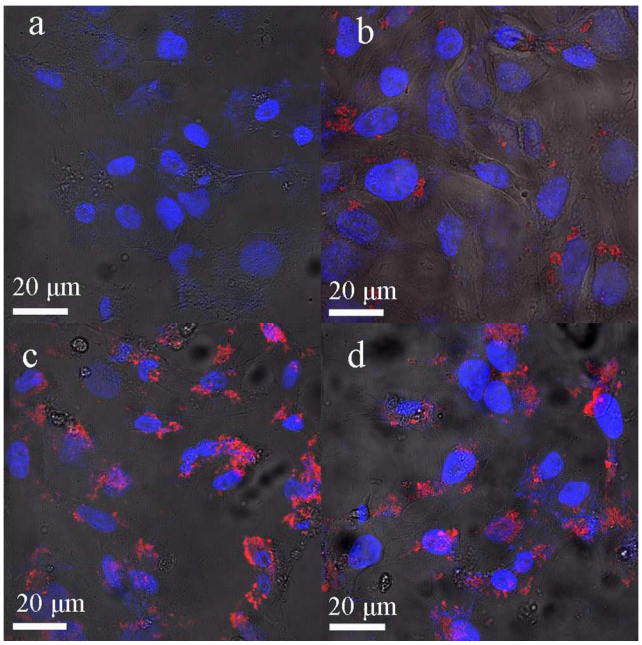


**Fig. 5** CLSM images of KHOS cells after incubation for 4 h at 37°C alone (a) or with RB-SR-3.40 (b), RB-SR-3.88 (c) and RB-MCM-41 (d) (50μg $ml^{-1}$). The blue regions represent the signal from the nuclei and the red regions are the signal from RB.

To quantitatively compare the cellular uptake efficiency of SR-3.40, SR-3.88 and MCM-41, ICP-OES was used to determine the amount of silica nanoparticles internalized into KHOS cells. As shown in Fig. 6, SR-3.88 exhibit the highest cellular uptake performance (7.4 pg/cell), which is almost 4 times higher than that of SR-3.40 (2.0 pg/cell) and slightly higher than that of MCM-41 (6.1 pg/cell). This result is consistent with CLSM observation. The slight enhancement in cell internalization of SR-3.88 compared to MCM-41 could be attributed to its larger aspect ratio. [28]

Nanocarriers should be biocompatible in their biomedical applications, thus the low cytototoxicity of SR-3.88 is crucial.

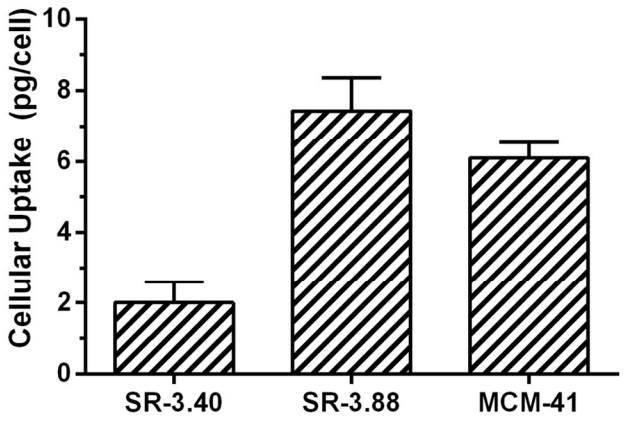


**Fig. 6** Cell uptake of SR-3.40, SR-3.88 and MCM-41. The Y axis is the mass of silicon per cell.

The biocompability of SR-3.88 was evaluated in KHOS cells by MTT assay and compared with the most extensively studied nanocarrier, MCM41. Fig. S3 shows the KHOS cells viability in the presence of SR-3.88 or MCM41 after 24 h incubation. SR-3.88 exhibits excellent biocompatibility up to the concentration as high as 200 μg $ml^{-1}$ while MCM-41 causes 25% cell death at this dose.

## 4. Conclusions

A facial approach was developed to synthesize SBA-15 rods with 80-200 nm in length and 18±8 nm in width by precisely controlling pH value in the range of 3.40-3.88. The small-sized SBA-15 rods show improved adsorption capacity towards bovine serum albumin and lysozyme than those of large SBA-15 rods and conventional MCM-41, attributed to its smaller particle sizes and relatively larger pore sizes, respectively. Moreover, the small SBA-15 rods exhibit highly enhanced cellular uptake efficiency, which is almost 4 times higher than that of large ones and slightly higher than that of MCM-41with small sizes. The developed novel SBA-15 rods with small sizes are expected as promising nano-carriers for cellular delivery of various large biomolecules, such as therapeutic proteins or genetic molecules.

## Acknowledgment

We acknowledge the support from the Australian Research Council, the Cancer Council of Queensland, the Queensland Government, the Australian National Fabrication Facility and the Australian Microscopy and Microanalysis Research Facility at the Centre for Microscopy and Microanalysis, The University of Queensland.

## Notes and references

[a] *Australian Institute for Bioengineering and Nanotechnology, The University of Queensland, Brisbane, QLD 4072, Australia.*
*Fax: +61 7 3346 3973; Tel: +61 7 3346 3283; E-mail: c.yu@uq.edu.au*
[b] *Queensland Alliance for Agriculture and Food Innovation, The University of Queensland, Australia.*

† Electronic Supplementary Information (ESI) available: [details of any supplementary information available should be included here]. See DOI: 10.1039/b000000x/

‡ These authors contribute equally to this paper .

1. J. Kim, Y. Piao and T. Hyeon, *Chem. Soc. Rev.*, 2009, 38, 372-390.
2. F. Q. Tang, L. L. Li and D. Chen, *Adv. Mater.*, 2012, 24, 1504-1534.
3. A. Schulz and C. McDonagh, *Soft Matter*, 2012, 8, 2579-2585.
4. C. T. Kresge, M. E. Leonowicz, W. J. Roth, J. C. Vartuli and J. S. Beck, *Nature*, 1992, 359, 710-712.
5. F. Lu, S. H. Wu, Y. Hung and C. Y. Mou, *Small*, 2009, 5, 1408-1413.
6. Slowing, II, J. L. Vivero-Escoto, C. W. Wu and V. S. Y. Lin, *Adv. Drug Deliv.Rev.*, 2008, 60, 1278-1288.
7. H. I. Lee, J. H. Kim, G. D. Stucky, Y. F. Shi, C. Pak and J. M. Kim, *J. Mater. Chem.*, 2010, 20, 8483-8487.
8. D. Y. Zhao, J. L. Feng, Q. S. Huo, N. Melosh, G. H. Fredrickson, B. F. Chmelka and G. D. Stucky, *Science*, 1998, 279, 548-552.
9. L. V. Carvalho, R. D. Ruiz, K. Scaramuzzi, E. B. Marengo, J. R. Matos, D. V. Tambourgi, M. C. A. Fantini and O. A. Sant'Anna, *Vaccine*, 2010, 28, 7829-7836.
10. H. Vallhov, N. Kupferschmidt, S. Gabrielsson, S. Paulie, M. Stromme, A. E. Garcia-Bennett and A. Scheynius, *Small*, 2012, 8, 2116-2124.
11. L. P. Mercuri, L. V. Carvalho, F. A. Lima, C. Quayle, M. C. A. Fantini, G. S. Tanaka, W. H. Cabrera, M. F. D. Furtado, D. V. Tambourgi, J. D. R. Matos, M. Jaroniec and O. A. Sant'Anna, *Small*, 2006, 2, 254-256.
12. J. Fan, J. Lei, L. M. Wang, C. Z. Yu, B. Tu and D. Y. Zhao, *Chem. Commun.*, 2003, 2140-2141.
13. C. Z. Yu, J. Fan, B. Z. Tian, D. Y. Zhao and G. D. Stucky, *Adv. Mater.*, 2002, 14, 1742-1745.
14. A. Sayari, B. H. Han and Y. Yang, *J.Am.Chem. Soc.*, 2004, 126, 14348-14349.
15. X. L. Ji, K. T. Lee, M. Monjauze and L. F. Nazar, *Chem. Commun.*, 2008, 4288-4290.
16. E. M. Johansson, M. A. Ballem, J. M. Cordoba and M. Oden, *Langmuir*, 2011, 27, 4994-4999.
17. Y. Ding, G. F. Yin, X. M. Liao, Z. B. Huang, X. C. Chen, Y. D. Yao and J. Li, *Micropor. Mesopor. Mater.*, 2013, 170, 45-51.
18. S. Yang, L. Z. Zhao, C. Z. Yu, X. F. Zhou, J. W. Tang, P. Yuan, D. Y. Chen and D. Y. Zhao, *J. Am. Chem. Soc.*, 2006, 128, 10460-10466.
19. S. L. Isley and R. L. Penn, *J. Phys. Chem. C*, 2008, 112, 4469-4474.
20. D. Y. Zhao, Q. S. Huo, J. L. Feng, B. F. Chmelka and G. D. Stucky, *J. Am. Chem. Soc.*, 1998, 120, 6024-6036.
21. Y. Wan, Y. F. Shi and D. Y. Zhao, *Chem. Commun.*, 2007, 897-926.
22. H. N. Wang, Y. H. Wang, X. Zhou, L. Zhou, J. Tang, J. Lei and C. Yu, *Adv. Funct. Mater.*, 2007, 17, 613-617.
23. P. Yuan, S. Yang, H. N. Wang, M. H. Yu, X. F. Zhou, G. Q. Lu, J. Zou and C. Z. Yu, *Langmuir*, 2008, 24, 5038-5043.
24. S. Hudson, J. Cooney and E. Magner, *Angew. Chem. Int. Edit.*, 2008, 47, 8582-8594.
25. J. Deere, E. Magner, J. G. Wall and B. K. Hodnett, *J. Phys. Chem. B*, 2002, 106, 7340-7347.
26. A. Katiyar and N. G. Pinto, *Small*, 2006, 2, 644-648.
27. A. Vinu, V. Murugesan and M. Hartmann, *J. Phys. Chem. B*, 2004, 108, 7323-7330.
28. H. Meng, S. Yang, Z. X. Li, T. Xia, J. Chen, Z. X. Ji, H. Y. Zhang, X. Wang, S. J. Lin, C. Huang, Z. H. Zhou, J. I. Zink and A. E. Nel, *Acs Nano*, 2011, 5, 4434-4447.